

Dynamic Modeling of Cytochrome P450 Inhibition In Vitro: Impact of Inhibitor Depletion on IC₅₀ Shift[§]

Loren M. Berry, Zhiyang Zhao, and Min-Hwa Jasmine Lin

Pharmacokinetics and Drug Metabolism, Amgen, Inc., Cambridge, Massachusetts

Received February 8, 2013; accepted May 2, 2013

ABSTRACT

The impact of inhibitor depletion on the determination of shifted IC₅₀ (IC₅₀ determined after 30 minutes of preincubation with inhibitor) is examined. In addition, IC₅₀-shift data are analyzed using a mechanistic model that incorporates the processes of inhibitor depletion, as well as reversible and time-dependent inhibition. Anomalies such as a smaller-than-expected shift in IC₅₀ and even increases in IC₅₀ with preincubation were explained by the depletion of inhibitor during the preincubation. The IC₅₀-shift assay remains a viable approach to characterizing a wide range of reversible and time-dependent inhibitors. However, as with more traditional time-dependent inactivation methods, it is recommended that IC₅₀-shift experimental data be interpreted with some

knowledge of the magnitude of inhibitor depletion. For the most realistic classification of time-dependent inhibitors using IC₅₀-shift methods, shifted IC₅₀ should be calculated using observed inhibitor concentrations at the end of the incubation rather than nominal inhibitor concentrations. Finally, a mechanistic model that includes key processes, such as competitive inhibition, enzyme inactivation, and inhibitor depletion, can be used to describe accurately the observed IC₅₀ and shifted IC₅₀ curves. For compounds showing an IC₅₀ fold shift >1.5 based on the observed inhibitor concentrations, reanalyzing the IC₅₀-shift data using the mechanistic model appeared to allow for reasonable estimation of K_i , K_I , and k_{inact} directly from the IC₅₀ shift experiments.

Introduction

Previously, we described an IC₅₀ and IC₅₀-shift assay for simultaneously determining reversible inhibition potency and classifying reversible and time-dependent inhibitors of CYP3A4, CYP2C9, and CYP2D6 (Berry and Zhao, 2008). The methods avoided the secondary dilution step found in most traditional approaches to identifying time-dependent inhibitors and was able successfully to characterize noninhibitors, reversible inhibitors, and time-dependent inhibitors among a wide range of reference and proprietary compounds. Others have also described successful applications of IC₅₀-shift style assays in various forms (Obach et al., 2007; Grimm et al., 2009; Perloff et al., 2009; Burt et al., 2010). In addition, both empirical and mechanistic relationships were explored that examine the link between enzyme inactivation and IC₅₀ shift and validate the principle and application of the IC₅₀-shift approach to characterizing cytochrome P450 (P450) inhibition (Maurer et al., 2000; Berry and Zhao, 2008; Krippendorff et al., 2009).

Since establishing and implementing such assays, some anomalies have been observed. In particular, some investigators have noted that the magnitude of decrease in IC₅₀ after preincubation can at times appear to underestimate the extent of time-dependent inactivation observed during traditional K_I and k_{inact} experiments. For example, ritonavir is known to be a highly potent inactivator of CYP3A4 (Kirby et al., 2011), yet it yields relatively little shift in IC₅₀ with preincubation (Obach et al., 2007; Berry and Zhao, 2008). In addition, cases have been observed where the IC₅₀ can appear to increase after

preincubation, as occurs with the nicardipine IC₅₀ against CYP2C9 (Berry and Zhao, 2008). Such examples have added some uncertainty to the interpretation of IC₅₀-shift data in terms of classifying time-dependent inhibitors. It is often suggested that the main culprit behind these anomalies is the metabolism of inhibitor during the incubation; however, the impact of inhibitor depletion on the shifted IC₅₀ has not been investigated, and that is an aim of the present study.

Historically, the best practices to determine enzyme kinetics accurately, including inhibition kinetics, call for keeping the incubations short such that less than 10% of substrate or inhibitor is depleted. Experiments to determine time-dependent inhibition, including traditional dilution methods, as well as IC₅₀-shift experiments, could potentially violate this guideline. This is because preincubation with inhibitor often must be carried out for as long as 30 minutes (or longer depending on the inhibitor) to observe the time dependency in inhibition (Grimm et al., 2009). Furthermore, mechanism-based inactivation requires at least partial conversion of the inhibitor to a bioreactive metabolite or intermediate. Thus, the apparent kinetics of inactivation relative to nominal inhibitor concentrations could change over the course of preincubation as inhibitor is depleted. Previously reported mechanistic relationships that attempt to describe IC₅₀ shift do not account for inhibitor depletion; therefore, we developed a dynamic model to describe IC₅₀-shift style data that consider inhibitor depletion, as well as reversible inhibition and enzyme activation. We anticipate that the proposed model will be useful for providing more robust characterization of P450 inhibitors in vitro.

dx.doi.org/10.1124/dmd.113.051508.

[§]This article has supplemental material available at dmd.aspetjournals.org.

ABBREVIATIONS: LC-MS/MS, liquid chromatography-tandem mass spectrometry; MPA, mobile phase A; MPB, mobile phase B; m/z , mass-to-charge ratio; P450, cytochrome P450.

Materials and Methods

All compounds and solvents were obtained from commercial sources as appropriate. Pooled human liver microsomes (pool of 50 donors) were obtained from Gibco (Life Technologies Co., Grand Island, NY).

Determination of Metabolite Formation Kinetics. Kinetics for the formation of 1-hydroxymidazolam, 4'-hydroxydiclofenac, and dextropran from the substrates midazolam, diclofenac, and dextromethorphan, respectively, were determined in preliminary experiments. Substrates were incubated at 37°C for 5 minutes at a concentration range of 0.2–50 μM, in the presence of 0.1 mg of human liver microsomal protein per milliliter, 1 mM NADPH, and 50 mM potassium phosphate buffer, pH 7.4 (300 μl total incubation volume). At the end of the incubation period, samples were collected into an equal volume of acetonitrile containing the internal standards (the stable isotopes of the marker metabolites), and the mixtures were centrifuged and analyzed on an liquid chromatography-tandem mass spectrometry (LC-MS/MS) system for the marker metabolites and internal standards. Resulting analyte/internal standard peak area ratios were converted to concentration by means of comparison with a calibration curve of marker metabolite and internal standard prepared in the same matrix as the samples. Metabolite concentrations were converted to reaction velocity [$v = C_{\text{form}}/(\text{incubation time} \cdot \text{microsomal protein concentration})$]. $V_{\text{max},f}$ and $K_{m,f}$ were estimated from the velocity versus substrate concentration data using GraphPad Prism version 5 (GraphPad Software Inc., San Diego, California) assuming Michaelis-Menten kinetics.

IC₅₀ and IC₅₀-Shift with Inhibitor Depletion. Inhibition of CYP3A4, CYP2D6, and CYP2C9 was assessed in 96-well format with a TECAN Freedom Evo automated workstation (TECAN Inc., Durham, NC), optimized for pipetting accuracy and precision. Test inhibitors were predissolved in 50% acetonitrile and 50% water (5 mM) and stored at -80°C until use. All incubation solutions (300 μl) contained 0.1 mg of human microsomal protein per milliliter and 1 mM NADPH in 50 mM potassium phosphate buffer, pH 7.4. The timeline of the incubation was as follows: In the presence of NADPH, test inhibitors (0 μM plus seven concentrations, depending on the inhibitor) were added to the 37°C incubations either at 0 minutes of incubation (for preincubation with inhibitor, shifted IC₅₀ determinations) or at 30 minutes of incubation (for IC₅₀ determinations). Each compound was tested in duplicate. Marker substrate cocktail was added to all incubations at 30 minutes. Addition of the marker substrate cocktail yielded the final substrate concentrations of 3 μM midazolam, 7 μM diclofenac, and 6 μM dextromethorphan. These concentrations are near the measured Michaelis-Menten constant (K_m) values for these marker reactions under the incubation conditions used here (Table 1). The addition of inhibitor or substrate did not significantly dilute the incubation mixture (i.e., ~5% dilution). After addition of the marker substrate cocktail, the incubation proceeded for an additional 5 minutes (to 35 minutes of total incubation time). At the end of the incubation period, samples were collected into an equal volume of acetonitrile containing the internal standards (the stable isotopes of the marker metabolites), and the mixtures were centrifuged and analyzed on an LC-MS/MS system for the marker metabolites, internal standards, and inhibitor.

Inhibition of P450 activity in the presence of varying concentrations of test compound was calculated as the percent of remaining activity (%activity) in each sample relative to the control sample (plus NADPH, but without inhibitor). Values for IC₅₀ and shifted IC₅₀ were calculated from the %activity data by a four-parameter logistic model in Galileo v3.2 (Thermo Electron Corp., Madison, WI). IC₅₀ values were initially calculated using nominal inhibitor concentrations. To determine the impact of inhibitor

depletion on the apparent IC₅₀ fold shift, shifted IC₅₀ values were calculated using both nominal inhibitor concentrations and inhibitor concentrations present at the end of the 30-minute preincubation with inhibitor (observed inhibitor concentrations). IC₅₀ fold shift is the ratio of IC₅₀ divided by the shifted IC₅₀.

Analytical Procedure. Samples were analyzed by multiple reaction monitoring on an LC-MS/MS system consisting of dual Shimadzu LC-10AD high-performance liquid chromatography pumps and a DGU-14A degasser (Shimadzu, Columbia, MD), a CTC PAL autoinjector (Leap Technologies, Carboro, NC), and an API3000 LC-MS/MS system equipped with an electrospray ion source and operated by the Analyst software package (Applied Biosystems, Foster City, CA). Chromatography was conducted on a Sprite Armor C18 (20 × 2.1 mm, 10 μm) analytical column (Analytical Sales and Services, Pompton Plains, NJ) with a 0.5-μm PEEK guard filter, using the following mobile phase gradient program at a flow rate of 0.5 ml/min: mobile phase A (MPA) = H₂O with 0.1% formic acid; mobile phase B (MPB) = acetonitrile with 0.1% formic acid; 0 minutes = 98% MPA, 2% MPB; 0.8 minutes = 2% MPA, 98% MPB; 1.0 minute = 2% MPA, 98% MPB; 1.1 minutes = 98% MPA, 2% MPB; 1.2 minutes = end of run; approximately 1.5 minutes between sample injections. For the first 0.3 minutes of each sample run, 100% of the LC eluent was diverted from the ion source to waste, and ~50% was split to waste thereafter; 1'-hydroxymidazolam [mass-to-charge ratio (m/z) 342 → 324], 1'-hydroxymidazolam stable isotope (m/z 345 → 327), 4'-hydroxydiclofenac (m/z 312 → 230), 4'-hydroxydiclofenac stable isotope (m/z 318 → 236), dextropran (m/z 258 → 157), and dextropran stable isotope (m/z 261 → 157) were detected in positive ion mode.

Kinetic Modeling of P450 Inhibition. A mechanistic model for P450 inhibition in the IC₅₀-shift assay accounting for the metabolism of inhibitor, metabolism of substrate, and reversible and time-dependent loss of enzyme activity was created based on the scheme shown in Fig. 1.

The kinetics of inhibitor metabolism was determined based on the depletion of inhibitor in the incubation. Briefly, since all IC₅₀ and shifted IC₅₀ samples were incubated to 35 minutes, the inhibitor depletion rates could be determined by measuring the loss of inhibitor in the IC₅₀ samples (5 minutes of incubation with inhibitor) and the shifted IC₅₀ samples (35 minutes of incubation with inhibitor), relative to samples spiked with inhibitor but not incubated (0 minutes of incubation). Depletion of the inhibitor at each concentration is described by eq. 1:

$$V \cdot \frac{dC_{\text{inh}}}{dt} = -CL_{\text{int,inh}} \cdot C_{\text{inh}} \quad (1)$$

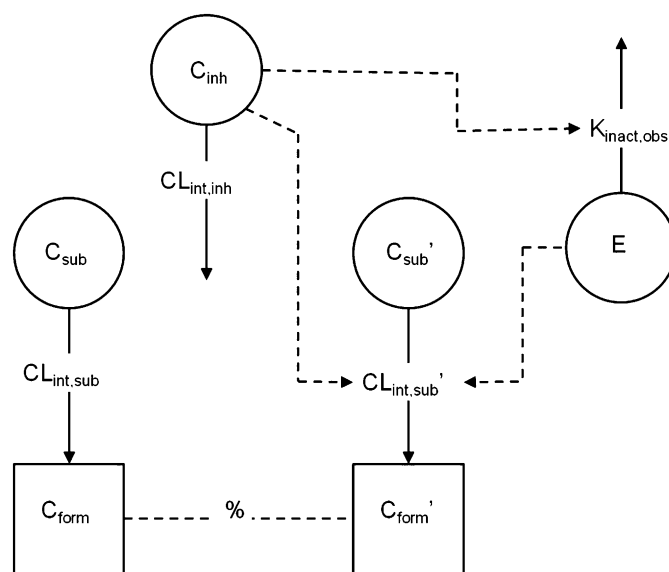


Fig. 1. Mechanistic model for P450 inhibition, including metabolism of inhibitor, metabolism of substrate, competitive inhibition, and time-dependent inactivation of enzyme.

TABLE 1

Michaelis-Menten kinetic parameters for the formation of 1-hydroxymidazolam, 4'-hydroxydiclofenac, and dextropran from midazolam, diclofenac, and dextromethorphan in human liver microsomes

	$V_{\text{max},f}$	$K_{m,f}$
	pmol/(min·mg)	μM
1-Hydroxymidazolam	656 ± 23	2.83 ± 0.19
4'-Hydroxydiclofenac	2600 ± 40	7.42 ± 0.30
Dextropran	129 ± 4	6.34 ± 0.46

where C_{inh} is the concentration of inhibitor in the incubation, V is the volume of the incubation per milligram of microsomal protein, and $CL_{int,inh}$ is the intrinsic clearance of the inhibitor. When $CL_{int,inh}$ was observed to be concentration dependent over the concentration range tested, it was as shown in eq. 2:

$$CL_{int,inh} = \frac{V_{max,inh}}{K_{m,inh} + C_{inh}} + CL_{int,us} \quad (2)$$

assuming the concentration dependence in inhibitor depletion is reasonably described by Michaelis-Menten style kinetics with or without an additional unsaturable component, where $V_{max,inh}$ is the apparent maximum reaction velocity for the depletion of inhibitor, $K_{m,inh}$ is the apparent concentration of inhibitor required to achieve 50% of $V_{max,inh}$, and $CL_{int,us}$ is the component of intrinsic clearance that is unsaturable over the concentration range tested (when applicable). For further discussion purposes, $V_{max,inh}$, $K_{m,inh}$, and $CL_{int,us}$ were used to calculate $CL_{int,max}$, representing the maximum intrinsic clearance observed for the inhibitor, typically at the lowest concentrations tested. $CL_{int,max}$ equals $CL_{int,us}$ for those inhibitors with no observed concentration dependence over the concentration range tested (e.g., troleandomycin). $CL_{int,max}$ equals $V_{max,inh}/K_{m,inh}$ for inhibitors with apparently only a saturable component. $CL_{int,max}$ equals $V_{max,inh}/K_{m,inh} + CL_{int,us}$ for those inhibitors with both saturable and unsaturable components over the concentration range tested (e.g., delavirdine).

Time-dependent inactivation of P450 enzyme is defined by eq. 3:

$$\frac{dE}{dt} = -k_{obs} \cdot E \quad (3)$$

where E represents the fraction of active P450 enzyme. At the beginning of the incubation and in the absence of inhibitor, E equals 1; k_{obs} is the rate of inactivation of enzyme and is dependent on the concentration of inhibitor such that, as shown in eq. 4:

$$k_{obs} = \frac{k_{inact} \cdot C_{inh}}{K_I + C_{inh}} \quad (4)$$

where k_{inact} is the maximum rate of inactivation and K_I is the concentration required to achieve 50% of k_{inact} .

Since in human liver microsomes midazolam, diclofenac, and dextromethorphan are selective substrates for CYP3A4, CYP2C9, and CYP2D6, respectively, and each only forms one primary metabolite, the rate of metabolite formation was assumed to equal the rate of substrate depletion. Additionally, the metabolites formed are assumed not to be subject to further metabolism under the incubation conditions used. As shown in eqs. 5 and 6, in the absence of inhibitor, the concentration of metabolite formed from the substrate is also considered to be driven by Michaelis-Menten kinetics and forms such that

$$V \cdot \frac{dC_{form}}{dt} = CL_{int,f} \cdot C_{sub} = -V \cdot \frac{dC_{sub}}{dt} \quad (5)$$

and

$$CL_{int,f} = \frac{V_{max,f}}{K_{m,f} + C_{sub}} \quad (6)$$

where C_{sub} is the concentration of substrate remaining in the absence of inhibitor; C_{form} is the concentration of metabolite formed in the absence of inhibitor; and $CL_{int,f}$, $V_{max,f}$, and $K_{m,f}$ are the intrinsic clearance, maximal reaction velocity, and concentration required to reach 50% of $V_{max,f}$ for the formation of metabolite in the absence of inhibitor. Values used in the equations for $V_{max,f}$ and $K_{m,f}$ were determined in preliminary experiments and are shown in Table 1. As shown in eqs. 7 and 8, in the presence of inhibitor, metabolite formation is expected to be altered by immediate reversible (i.e., competitive) inhibition, as well as by time-dependent (i.e., quasi-irreversible or irreversible) inactivation such that

$$V \cdot \frac{dC_{form}'}{dt} = CL_{int,f}' \cdot C_{sub}' = -V \cdot \frac{dC_{sub}'}{dt} \quad (7)$$

and

$$CL_{int,f}' = \frac{V_{max,f} \cdot E}{K_{m,f} \left(1 + \frac{C_{inh}}{K_i}\right) + C_{sub}'} \quad (8)$$

where C_{sub}' is the concentration of substrate remaining, C_{form}' is the concentration of metabolite formed, $CL_{int,f}'$ is the intrinsic formation clearance in the presence of inhibitor, and K_i is the inhibition constant for the competitive inhibition. As shown in eq. 9, at each dose of inhibitor, inhibition results are expressed as the percentage of enzyme activity remaining in the presence of inhibitor relative that in the absence of inhibitor:

$$\%Activity = 100 \cdot \frac{C_{form}'}{C_{form}} \quad (9)$$

Model equations were programmed into Phoenix version 6.3 (Certara L.P., St. Louis, MO) as a textual model (see Supplemental Material). To mimic the conditions used for in vitro IC_{50} and IC_{50} shift experiments, doses of inhibitor were given at 0 minutes (for preincubation with inhibitor, shifted IC_{50} samples) or at 30 minutes (for preincubation without inhibitor, IC_{50} samples). Doses of substrate were given at 30 minutes. Each dose level and dose time of inhibitor was treated as a unique subject, for a total of 16 subjects. Model equations were solved for $V_{max,inh}$, $K_{m,inh}$, K_i , K_I , and k_{inact} in population mode using the observed values for C_{inh} and $\%Activity$ after 35 minutes of total incubation time (5 minutes of incubation with substrate).

Results

IC_{50} and IC_{50} Shift. IC_{50} and shifted IC_{50} values for a number of inhibitors are shown in Table 2. Shifted IC_{50} was initially calculated using nominal inhibitor concentrations. Using nominal inhibitor concentrations, a few well known potent inactivators of CYP3A4, CYP2C9, or CYP2D6 showed a substantial (>10-fold shift) decrease in IC_{50} after preincubation, including delavirdine/CYP3A4, mibefradil/CYP3A4, mifepristone/CYP3A4, paroxetine/CYP2D6, and tienilic acid/CYP2C9. A number of well-known inactivators also showed more moderate (1.5-fold to 10-fold shift) decreases in IC_{50} after preincubation, including dasatinib/CYP3A4, delavirdine/CYP2D6, erythromycin/CYP3A4, nicardipine/CYP3A4, and troleandomycin/CYP3A4. Several inhibitors showed minimal (0.7- to 1.5-fold) shift in IC_{50} , including delavirdine/CYP2C9, ritonavir/CYP3A4, and saquinavir/CYP3A4. Finally, several inhibitors tested showed an increase (<0.7-fold shift) in IC_{50} after preincubation, including ketoconazole/CYP3A4, nicardipine/CYP2C9, and nicardipine/CYP2D6.

Since some unusual results were observed, including a lack of IC_{50} shift with known CYP3A4 inactivators ritonavir and saquinavir and increases in IC_{50} after preincubation with ketoconazole and nicardipine, it was hypothesized that depletion of inhibitor (as well as enzyme inactivation and incubation time) could influence the shifted IC_{50} . To understand the impact of possible inhibitor depletion on shifted IC_{50} , the shifted IC_{50} values were recalculated using the inhibitor concentrations observed at the end of the incubation. Based on observed inhibitor concentrations, several inhibitors yielded substantially reduced shifted IC_{50} levels, including ketoconazole/CYP3A4, mifepristone/CYP3A4, nefazodone/CYP3A4, nicardipine, ritonavir/CYP3A4, and saquinavir/CYP3A4. Most dramatically, the CYP3A4 IC_{50} fold shift for nicardipine increased from 4.5-fold using nominal concentrations to 1750-fold using observed concentrations, CYP3A4 IC_{50} foldshift for ritonavir increased from 0.9-fold to 45.6-fold, and CYP3A4 IC_{50} fold shift for saquinavir increased from 0.5- to 15.2-fold. In addition, the CYP3A4 IC_{50} fold shift for ketoconazole increased from 0.6- to 1.3-fold, and the CYP2C9 IC_{50} fold shift for nicardipine increased from 0.2- to 1.2-fold. These data indicate that, in many cases, choice of inhibitor concentrations used to determine shifted IC_{50} (nominal versus observed) can influence the interpretation of the data.

TABLE 2

IC₅₀ (μM) based on nominal inhibitor concentrations (C_{inh}) and shifted IC₅₀ (μM) based on nominal or observed C_{inh}

Compound	P450	Nominal C _{inh}			Observed C _{inh}	
		IC ₅₀	Shifted IC ₅₀	Fold Shift	Shifted IC ₅₀	Fold Shift
Clarithromycin	CYP3A4	130	41.4	3.1	41.4	3.1
Dasatinib	CYP3A4	9.6	2.6	3.7	2.2	4.4
Delavirdine	CYP3A4	19.3	0.79	24.4	0.53	36.4
	CYP2C9	5.6	6.0	0.9	5.8	1.0
	CYP2D6	51.4	10.7	4.8	13.1	3.9
Diltiazem	CYP3A4	72.8	36.2	2.0	36.2	2.0
Erythromycin	CYP3A4	43.7	18.0	2.4	18.0	2.4
Ketoconazole	CYP3A4	0.013	0.021	0.6	0.0099	1.3
	CYP2C9	9.8	8.4	1.2	8.4	1.2
Mibefradil	CYP3A4	0.42	0.029	14.5	0.0076	55.3
	CYP2D6	1.2	0.51	2.4	0.46	2.6
Mifepristone	CYP3A4	5.0	0.43	11.6	0.12	41.7
	CYP2C9	4.9	2.7	1.8	1.3	3.8
	CYP2D6	7.1	16.3	0.4	12.5	0.6
Nefazodone	CYP3A4	2.1	0.23	9.1	0.0033	636
	CYP2C9	23.3	32.8	0.7	28.0	0.8
Nicardipine	CYP3A4	0.49	0.11	4.5	0.00028	1750
	CYP2C9	0.35	1.7	0.2	0.30	1.2
	CYP2D6	1.5	6.2	0.2	2.8	0.5
Paroxetine	CYP2D6	0.9	0.037	24.6	0.024	37.9
Ritonavir	CYP3A4	0.0082	0.0090	0.9	0.00018	45.6
	CYP2C9	2.0	2.2	0.9	2.2	0.9
	CYP2D6	1.0	2.9	0.3	2.9	0.3
Saquinavir	CYP3A4	0.50	1.0	0.5	0.033	15.2
	CYP2C9	29.2	33.9	0.9	31.2	0.9
	CYP2D6	8.4	8.5	1.0	3.5	2.4
Tienilic acid	CYP2C9	0.90	0.072	12.5	0.018	50.0
Troleandomycin	CYP3A4	4.7	1.1	4.3	0.19	24.7
Verapamil	CYP3A4	21.7	7.2	3.0	6.5	3.3

Dynamic Modeling of P450 Inhibition. Since shifted IC₅₀ appears to depend on the depletion of inhibitor as well as enzyme inactivation and incubation time, it was hypothesized that a more mechanistic approach to modeling IC₅₀ and shifted IC₅₀ curves could further explain the anomalies and provide more robust and meaningful information about P450 inhibition. The model developed incorporated metabolism kinetics of both inhibitor and substrate, as well as the contribution of both competitive inhibition- and time-dependent inactivation; and the timelines of dosing of inhibitor and substrate in the model were matched to that in the in vitro experiments. The best-fit values for the apparent V_{max} and K_m of the model parameters for depletion of the inhibitor are given in Table 3. Also calculated are the

inhibitor CL_{int,max} values, which represent the rates of depletion at the lowest concentrations tested. Depletion of many inhibitors was remarkably rapid, particularly at low concentrations, whereas the values for apparent K_m were often very low (~1 μM or lower). Therefore, saturation of metabolism was observed at the higher concentrations tested, typically preventing or minimizing depletion of inhibitor at the higher concentrations tested. This finding suggests that the calculation of shifted IC₅₀ would be influenced mostly by the depletion of inhibitor at low, unsaturating concentrations and confirms that accurate characterization of P450 inhibition kinetic parameters for many of the inhibitors tested requires consideration of inhibitor depletion kinetics.

TABLE 3

Apparent V_{max} and Michaelis-Menten dissociation constant (K_m) for the depletion of various P450 inhibitors

	V _{max}	K _m	CL _{int,us}	CL _{int,max}	Concentration Range
	pmol/(min/mg)	μM	μl/(min/mg)	μl/(min/mg)	μM
Clarithromycin	21.7 ± 8.1	0.509 ± 0.248		42.6	0.069–50
Dasatinib	194 ± 23	0.844 ± 0.116		230	0.069–50
Delavirdine	189 ± 20	0.651 ± 0.083	17.0 ± 7.9	307	0.069–50
Diltiazem	5122 ± 1056	77.3 ± 17.1		66.3	0.069–50
Erythromycin			28.9 ± 11.4	28.9	0.069–50
Ketoconazole	12.3 ± 5.1	0.0306 ± 0.0151		402	0.0014–1.0
Mibefradil	25.6 ± 5.4	0.0387 ± 0.0095		687	0.0027–2.0
Mifepristone	828 ± 218	1.59 ± 0.497		521	0.069–50
Nefazodone	1658 ± 122	1.16 ± 0.094		1429	0.014–10
Nicardipine	552 ± 56	0.273 ± 0.031		2022	0.0027–2.0
Paroxetine	13.4 ± 5.71	0.0535 ± 0.0297		250	0.0069–5.0
Ritonavir	18.9 ± 5.2	0.0126 ± 0.0019		1500	0.0014–1.0
Saquinavir	935 ± 28	0.558 ± 0.024		1676	0.069–50
Tienilic acid	42.4 ± 8.3	0.0589 ± 0.016		720	0.0069–5.0
Troleandomycin			611 ± 96	611	0.014–10
Verapamil	494 ± 77	2.33 ± 0.423		212	0.069–50

TABLE 4

Dynamic model fit parameters K_i , K_I , and k_{inact} from IC_{50} -shift experimental design considering kinetics of inhibitor depletion, compared with K_I and k_{inact} values determined from traditional experimental design and parameter fitting

Values are \pm S.E. or a range of values as appropriate.

Compound	P450	IC_{50} Shift by Substrate Addition (Fit with Dynamic Model)			Traditional Dilution Method (Range of Reference Values) ^a	
		K_i	K_I	k_{inact}	K_I	k_{inact}
		μM	μM	min^{-1}	μM	min^{-1}
Clarithromycin	CYP3A4	62.6 \pm 8.5	25.6 \pm 12.2	0.0204 \pm 0.0059	13.2–41.4	0.0192–0.063
Dasatinib	CYP3A4	5.25 \pm 0.71	1.17 \pm 0.39	0.0245 \pm 0.0044	2.6–6.3	0.024–0.034
Delavirdine	CYP3A4	14.5 \pm 2.1	1.45 \pm 0.85	0.0716 \pm 0.0079	3.8–15.9	0.056–0.29
	CYP2D6	15.9 \pm 1.5	3.34 \pm 0.97	0.0265 \pm 0.0030	3.89 \pm 1.07	0.0215 \pm 0.0030
Diltiazem	CYP3A4	23.2 \pm 5.2	1.76 \pm 0.85	0.00779 \pm 0.00227	0.48–18.1	0.005–0.019
Erythromycin	CYP3A4	20.7 \pm 2.3	5.27 \pm 2.19	0.0148 \pm 0.0034	1.7–17	0.017–0.081
Mibefradil	CYP3A4	0.297 \pm 0.038	0.0200 \pm 0.0033	0.0539 \pm 0.0045	0.13–2.3	0.042–0.7
	CYP2D6	0.410 \pm 0.040	0.161 \pm 0.054	0.0164 \pm 0.0031	1.09 \pm 0.31	0.0220 \pm 0.0021
Mifepristone	CYP3A4	3.59 \pm 0.67	0.308 \pm 0.041	0.0541 \pm 0.0040	0.61–1.6	0.061–0.091
	CYP2C9	1.83 \pm 0.31	1.86 \pm 0.88	0.0307 \pm 0.0096	None reported	
Nefazodone	CYP3A4	2.82 \pm 0.95	0.414 \pm 0.190	0.205 \pm 0.072	1.0–1.6	0.09–0.094
Nicardipine	CYP3A4	0.338 \pm 0.043	0.0424 \pm 0.0141	0.0864 \pm 0.0175	0.72–1.3	0.047–0.06
Paroxetine	CYP2D6	0.721 \pm 0.068	0.0789 \pm 0.0141	0.0790 \pm 0.0087	0.81–4.85	0.074–0.17
Ritonavir	CYP3A4	0.00456 \pm 0.00038	0.0527 \pm 0.0239	0.439 \pm 0.180	0.0106–0.5	0.05–0.45
Saquinavir	CYP3A4	0.251 \pm 0.027	0.484 \pm 0.167	0.0416 \pm 0.0091	1.54–5.9	0.026–0.0379
	CYP2D6	3.41 \pm 0.82	2.99 \pm 3.24	0.0388 \pm 0.0322	None reported	
Tienilic acid	CYP2C9	0.690 \pm 0.093	0.0969 \pm 0.0605	0.0840 \pm 0.0161	1.0–4.5	0.066–0.46
Troleandomycin	CYP3A4	2.42 \pm 0.14	0.271 \pm 0.047	0.0404 \pm 0.0025	0.19–2.4	0.032–0.171
Verapamil	CYP3A4	13.0 \pm 2.06	0.201 \pm 0.058	0.0260 \pm 0.0017	0.74–3.5	0.023–0.07

^a Reference values compiled from the following sources: Mayhew et al., 2000; Bertelsen et al., 2003; Ito et al., 2003; Zhao et al., 2005, 2007; Obach et al., 2007; Watanabe et al., 2007; Berry and Zhao, 2008; Perloff et al., 2009; Li et al., 2009; Mori et al., 2009; Xu et al., 2009; Kirby et al., 2011; Albaugh et al., 2012; Kenny et al., 2012; Amgen in-house data; University of Washington Drug Interaction Database (www.druginteractioninfo.org).

For compounds with an IC_{50} fold shift >1.5 based on observed inhibitor concentrations, best-fit values for K_i , K_I , and k_{inact} from the dynamic model are given in Table 4 and compared with available K_I and k_{inact} values gathered from various sources for reference. Several simulations are illustrated in more detail representing various effects of inhibitor depletion on the magnitude of IC_{50} shift. Erythromycin was not rapidly depleted during the incubation, with an average CL_{int} of 28.9 $\mu l/(min/mg)$ and showed moderate potency in the inactivation of CYP3A4 (Fig. 2A). The simulated and observed shifted IC_{50} curves were shifted to the left (more potent) relative to the simulated and observed IC_{50} curves, indicating time-dependent inactivation of

CYP3A4 (Fig. 2B). After the fitting of K_i , K_I , and k_{inact} , omitting inhibitor depletion by setting inhibitor V_{max} to zero in a subsequent simulation can help illustrate what the shifted IC_{50} curve might look like had inhibitor concentrations remained constant throughout the course of the incubation. In the case of erythromycin, omitting inhibitor depletion yielded minimal change in the simulated shifted IC_{50} curve (Fig. 2B) since depletion of inhibitor was initially slow.

Depletion of nicardipine was rapid and concentration dependent (Fig. 3A), whereas CYP3A4 inactivation was estimated to be rapid and nonlinear over the course of the incubation (Fig. 3B). The simulated and observed shifted IC_{50} curves were shifted to left (more

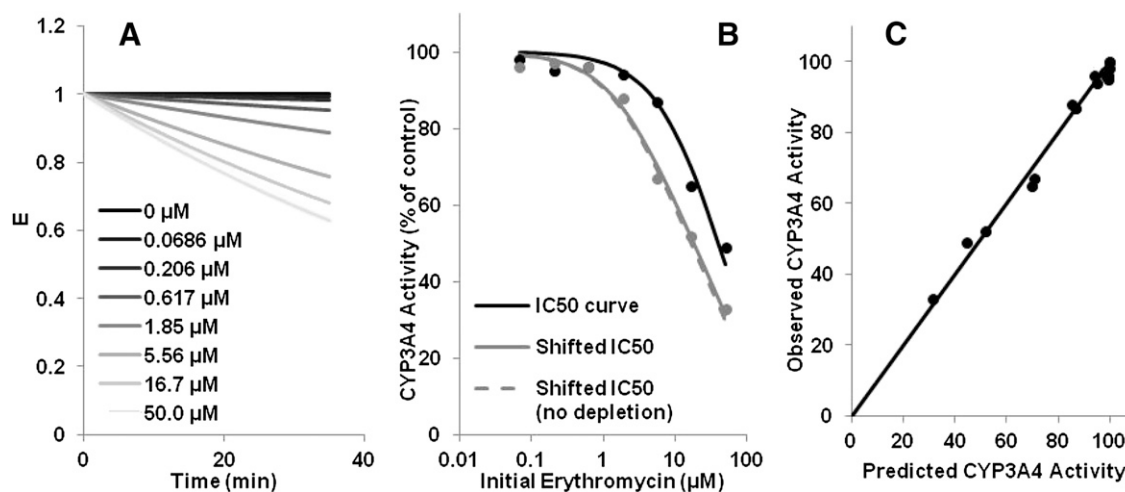


Fig. 2. Dynamic modeling of erythromycin IC_{50} shift. (A) Simulated time-dependent loss of CYP3A4 activity after preincubation with erythromycin. (B) Simulated (lines) and observed values (points) for CYP3A4 %Activity after preincubation with (shifted IC_{50}) or without (IC_{50}) erythromycin. Solid lines are simulations considering depletion of erythromycin. Dashed line is a simulated shifted IC_{50} curve without considering erythromycin depletion and using the fitted values for K_I and k_{inact} . (C) Model predicted versus observed values for %Activity. Depletion of erythromycin during the preincubation was minimal. E, represent the fraction of active P450 enzyme as defined by eq. 3.

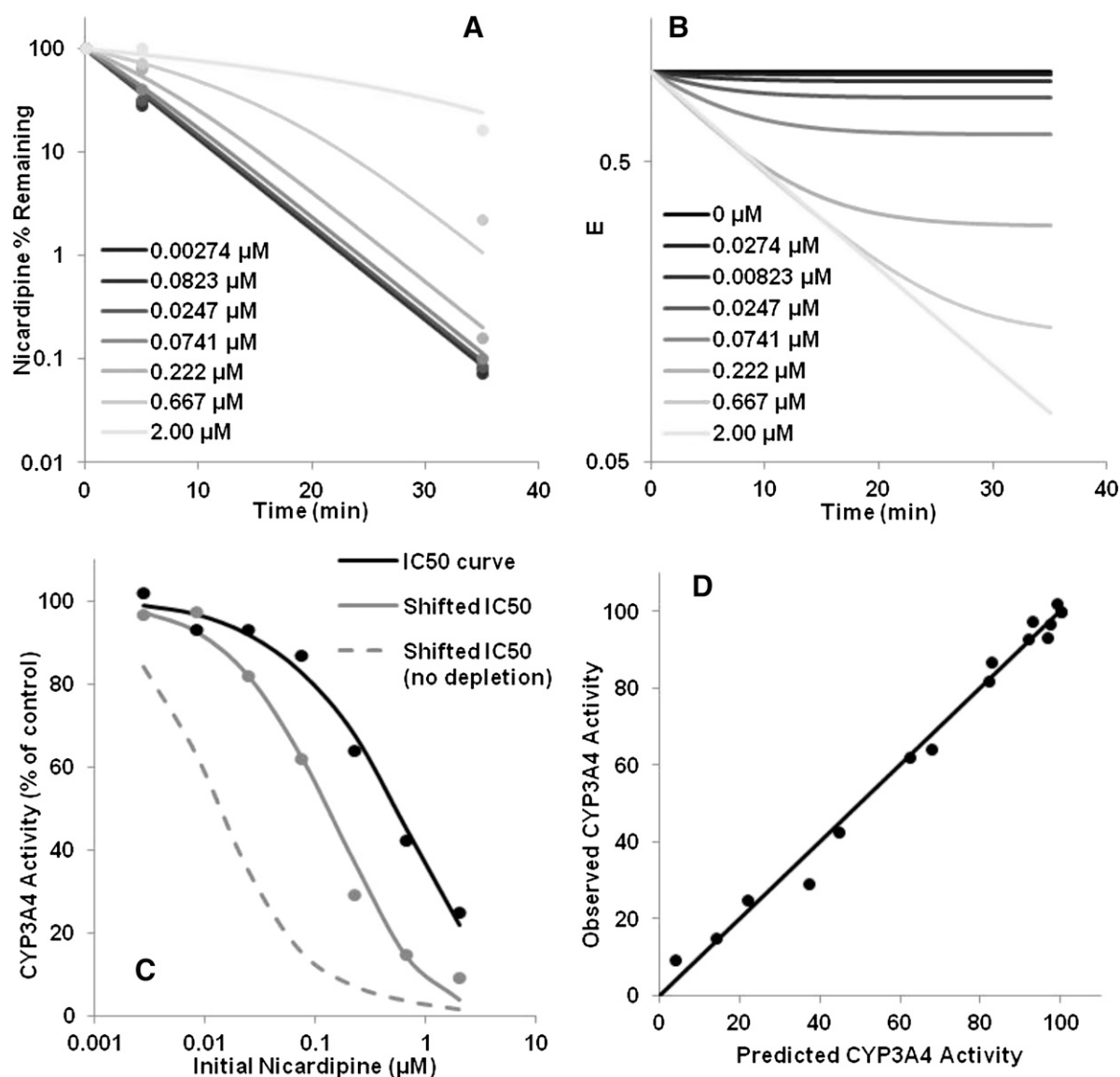


Fig. 3. Dynamic modeling of nicardipine IC_{50} shift. (A) Simulated (lines) and observed (points) depletion of nicardipine. (B) Simulated time-dependent loss of CYP3A4 activity after preincubation with nicardipine. (C) Simulated (lines) and observed values (points) for CYP3A4 %Activity after preincubation with (shifted IC_{50}) or without (IC_{50}) nicardipine. Solid lines are simulations considering depletion of nicardipine. Dashed line is a simulated shifted IC_{50} curve without considering nicardipine depletion and using the fitted values for K_I and k_{inact} . (D) Model predicted versus observed values for %Activity. E, represent the fraction of active P450 enzyme as defined by eq. 3.

potent) relative to the simulated and observed IC_{50} curves, indicating time-dependent inactivation of CYP3A4. However, omitting inhibitor depletion from the simulation yielded a more dramatic leftward shift in the shifted IC_{50} curve. In this case, it appears that depletion of inhibitor (and resulting loss of reversible and time-dependent inhibition) reduced the magnitude of the observed IC_{50} shift.

Depletion of saquinavir was also rapid and concentration dependent (Fig. 4A). However, despite relatively potent apparent CYP3A4 inactivation (Fig. 4B), the simulated and observed shifted IC_{50} curves were actually shifted to the right (less potent) relative to the simulated and observed IC_{50} curves (Fig. 4C). Omitting inhibitor depletion from the simulations resulted in a leftward shifted IC_{50} curve, as would be expected, given the CYP3A4 inactivation. It can be considered that depletion of inhibitor during the incubation (and loss of reversible inhibition) more than compensated for the CYP3A4 inactivation occurring during the incubation, particularly at the lowest concentrations.

Comparison of the K_I and k_{inact} values derived from the dynamic model versus the reference values is given in Table 4. Looking across a set of inhibitors with a wide range of potencies, k_{inact} values, derived from the dynamic model fit of the IC_{50} and shifted IC_{50} curves, appeared to fall within the range of available reference values or within 2-fold of the reference value when only one reference value was available. On the other hand, K_I values derived from the dynamic model tended to be more potent than the reference values. Since the traditional experimental methods used to determine the reference values often used higher microsomal protein concentrations than the dynamic IC_{50} shift method, we considered that some of the discrepancy in K_I values could be due to nonspecific microsomal binding. Therefore, K_I values were further corrected for microsomal binding at the protein concentrations used in the experiments. Correcting K_I values for microsomal binding by calculating unbound K_I ($K_{I,u}$) appeared to improve the correspondence between the dynamic model and the reference values (Fig. 5).

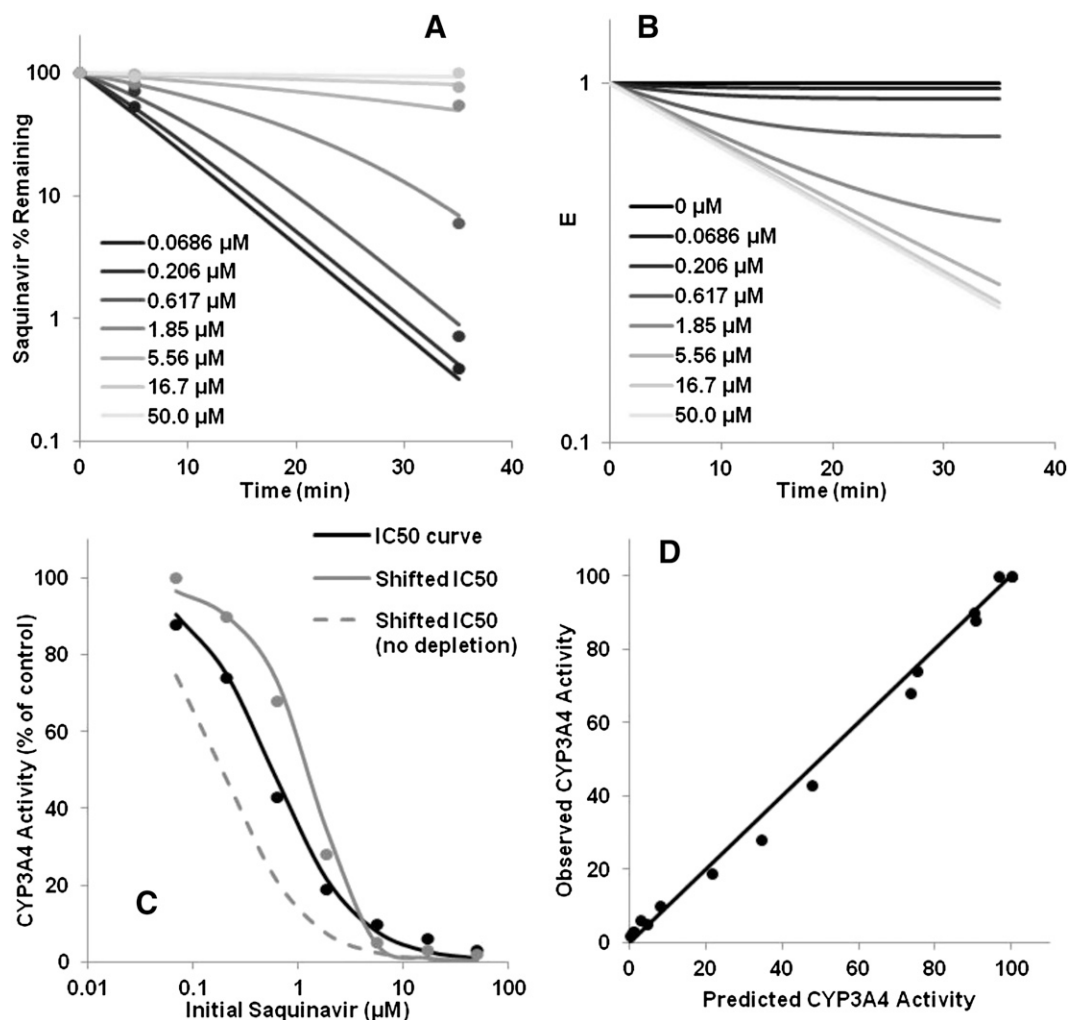


Fig. 4. Dynamic modeling of saquinavir IC₅₀ shift. (A) Simulated (lines) and observed (points) depletion of saquinavir. (B) Simulated time-dependent loss of CYP3A4 activity. (C) Simulated (lines) and observed values (points) for CYP3A4 %Activity after preincubation with (shifted IC₅₀) or without (IC₅₀) saquinavir. Solid lines are simulations considering depletion of saquinavir. Dashed line is a simulated shifted IC₅₀ curve without considering saquinavir depletion and using the fitted values for K_i and k_{inact} . (D) Model predicted versus observed values for %Activity. E, represent the fraction of active P450 enzyme as defined by eq. 3.

Discussion

In the present study, depletion of inhibitor was found to influence the apparent shifted IC₅₀ for many compounds. Although the widely used IC₅₀ and IC₅₀-shift-type assays can distinguish between reversible and time-dependent inhibitors in most cases, rapid depletion of inhibitor could cause a reduction in observed IC₅₀ fold shift or even an increase in IC₅₀ with preincubation time, potentially interfering with the classification of time-dependent inhibitors. A strong relationship exists between potential discrepancy in shifted IC₅₀ and $CL_{\text{int,max}}$ for the inhibitors tested (Fig. 6). Inhibitor depletion of 50% over the 30-minute preincubation with 0.1 mg of microsomal protein per milliliter equates to a CL_{int} of 230 $\mu\text{l}/(\text{min}\cdot\text{mg})$ and will result in a 2-fold increase in shifted IC₅₀. As $CL_{\text{int,max}}$ increases, the potential for discrepancy in shifted IC₅₀ increases exponentially. Therefore, the IC₅₀-shift assay is best interpreted with knowledge of inhibitor turnover, either from preliminary stability studies with human liver microsomes or by monitoring inhibitor depletion during the IC₅₀-shift experiment itself. Using observed inhibitor concentrations at the end of the 30-minute preincubation is likely to yield the most accurate assessment of IC₅₀ fold shift and the most realistic classification of time-dependent inhibitors, particularly for inhibitors with $CL_{\text{int,max}} > 230 \mu\text{l}/(\text{min}\cdot\text{mg})$.

Discrepancy in shifted IC₅₀ was also dependent on the saturation kinetics of inhibitor depletion. For some shifted IC₅₀ values, the discrepancy was not as large as expected given the $CL_{\text{int,max}}$ for the inhibitor. This was mainly the case for shifted IC₅₀ values greater than the apparent K_m for the depletion of inhibitor. If the shifted IC₅₀ $> K_m$, depletion of inhibitor at these concentrations and, therefore, discrepancy in shifted IC₅₀ is expected to be limited. However, if the IC₅₀ is near or below the apparent K_m , the discrepancy in shifted IC₅₀ could be pronounced. An example of this phenomenon is ritonavir. For ritonavir, shifted IC₅₀ values against CYP2C9 and CYP2D6 were similar whether calculated using nominal or observed concentrations, whereas the shifted IC₅₀ against CYP3A4 was substantially lower using observed concentrations. Since the phenomenon also appears to be dependent on the saturation kinetics of inhibitor depletion, it is important to evaluate inhibitor depletion over a range of concentrations to assess fully the impact of inhibitor depletion on shifted IC₅₀.

Although compared with IC₅₀ the shifted IC₅₀ is useful for the rapid classification of time-dependent inhibitor in vitro, we considered that it might not be the best measure of time-dependent inactivation potency. This is because the shifted IC₅₀ is dependent on the choice of inhibitor concentration used for its calculation (nominal versus observed), in addition to the extent of reversible inhibition and incubation

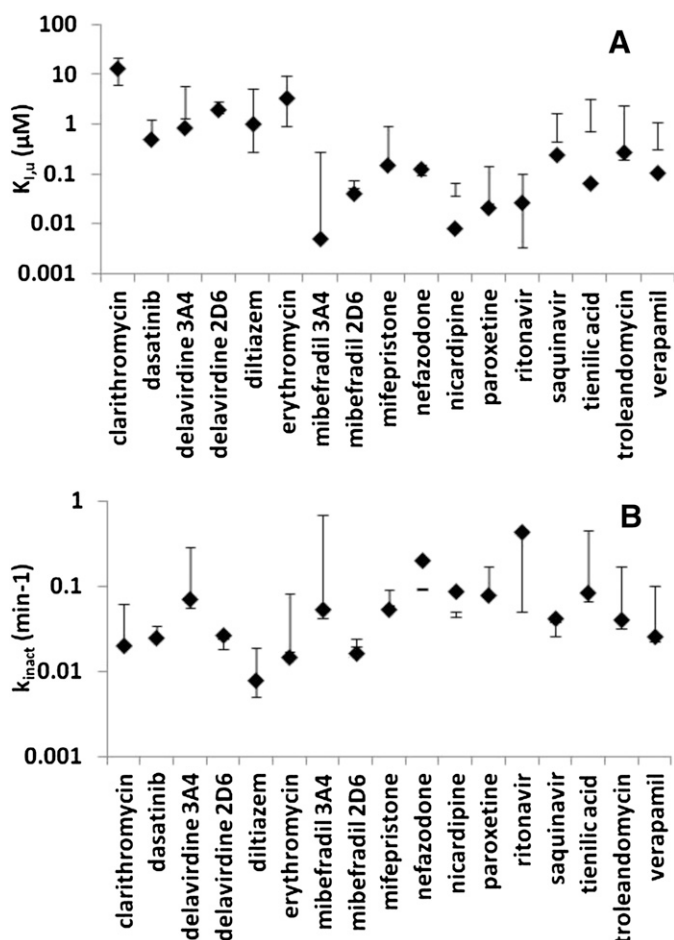


Fig. 5. Comparison of the $K_{I,u}$ (A) and k_{inact} (B) values determined from different methods. Bars represent the range of the available reference values, and points indicate values derived from the dynamic modeling. Values are for CYP3A4 inactivation unless otherwise noted. *Note:* Microsomal binding could not be determined for troleandomycin because of instability in microsomes; free fraction in microsomes is assumed to be 1 for troleandomycin.

time. Inhibition parameters K_I and k_{inact} have been more important in this regard, particularly in the application of extrapolation to in vivo drug-drug interactions. Therefore, a more complete mechanistic model was established to explain more fully the processes occurring in the IC_{50} -shift assay based on the scheme shown in Fig. 1 and applied to those inhibitors showing an IC_{50} fold shift >1.5 based on observed inhibitor concentrations. The model did a reasonable job of describing IC_{50} -shift data for all inhibitors, including those displaying anomalies in shifted IC_{50} discussed previously herein, such as nicardipine and saquinavir. It was also used to demonstrate the likely effect of inhibitor depletion on the shifted IC_{50} curves for erythromycin, nicardipine, and saquinavir. Inhibitor depletion caused a rightward shift in the shifted IC_{50} curves that opposes the leftward shift caused by enzyme inactivation. Combining the processes of inhibitor depletion and enzyme inactivation, the model was able to fit the fundamental parameters used in characterizing P450 inhibitors, $V_{max,inh}$, $K_{m,inh}$, K_I , K_I and k_{inact} , thereby definitively linking these process to observed shifts in the IC_{50} curves.

The model did a reasonable job of estimating $K_{I,u}$ and k_{inact} values for a wide range of inhibitors compared with reference values (Fig. 5). In a few cases, the $K_{I,u}$ determined by the dynamic modeling of IC_{50} and shifted IC_{50} curves appeared to be lower (more potent) than the

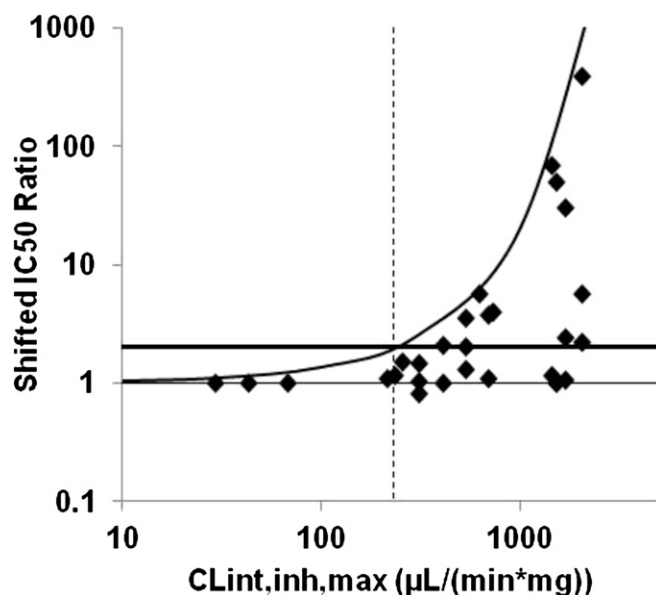


Fig. 6. Relationship between potential discrepancy in shifted IC_{50} versus inhibitor $CL_{int,inh,max}$. Shifted IC_{50} ratio is a measure of the discrepancy and equals shifted IC_{50} determined using nominal inhibitor concentrations divided by shifted IC_{50} determined using observed inhibitor concentrations. Solid horizontal lines are line of unity and a ratio of 2, respectively. Dashed vertical line represents a $CL_{int,inh,max}$ of $230 \mu L/(min \cdot mg)$. Curved line represents the maximum potential error in shifted IC_{50} for a given $CL_{int,inh,max}$.

available reference values, as was the case for nicardipine, saquinavir, and tienillic acid. The discrepancies could be due to interlaboratory variations, which have been quite large on occasion. They might also be explained by a “bias” in the K_I values determined by traditional experimental and parameter fitting methods, particularly when inhibitor depletion is rapid (Yang et al., 2005). Rapid inhibitor depletion causes nonlinearities in the enzyme inactivation profile over the course of the preincubation. An example from the present data set can be visualized in the inactivation of CYP3A4 by nicardipine (Fig. 3B). As nicardipine is depleted, the inactivation rate slows, particularly at low inhibitor concentrations, as it depends on the saturation kinetics of inhibitor depletion. In traditional approaches to fit inactivation parameters K_I and k_{inact} , depletion of inhibitor is typically assumed to be minimal. Even so, best practices have called for using only the initial observed rate of inactivation (k_{obs}) at each inhibitor concentration in the subsequent fitting of K_I and k_{inact} . Choosing which time points to consider becomes a judgment made by each individual scientist. In practice, it might be difficult to resolve the initial brief inactivation from the subsequent nonlinearity because of the lack of intensity of sampling or error resulting from sample dilution or analysis. Therefore, the k_{obs} may often be underestimated at low concentrations. The ultimate effect is a bias that overestimates the K_I value when inhibitor depletion is rapid. Mechanistic approaches to fitting K_I and k_{inact} in inactivation experiments have been proposed to help reduce such bias and provide more accurate characterization of these parameters (Yang et al., 2007). Hence, application of a mechanistic approach that incorporates inhibitor depletion should also provide more robust characterization of inhibitors using IC_{50} -shift methods.

The processes occurring in in vitro experiments to characterize P450 inhibition are clearly complex. In practice, assumptions are made to simplify the interpretation of P450 inhibition results. However, the present data set further demonstrates that the assumption regarding minimal inhibitor depletion is often not realistic and can dramatically impact interpretation of the data. Therefore, one can and should take

reasonable steps to account for depletion of inhibitor during time-dependent inactivation experiments, including IC_{50} -shift assays. Additional processes may be of some importance in both IC_{50} -shift and traditional dilution methods. First, in the present model, we have assumed that inhibitor depletion kinetics can be reasonably estimated using Michaelis-Menten kinetics. In reality, the contribution of substrate or product-dependent inhibition, as well as time-dependent autoinactivation, cannot be ruled out. Despite the limitation, the current model does a reasonable job of describing inhibitor concentrations over the course of the incubations, given the current data set (see Figs. 2–4 for examples). The current model, which incorporates inhibitor depletion kinetics (even in a simplified form), can be used to explain mechanistically the anomalies (reduced IC_{50} shift or increased IC_{50} with preincubation) described already. We therefore consider that the present model represents an improvement over previously reported models that neglect inhibitor depletion. Second, the ability of metabolites formed from the depletion of inhibitor to inhibit P450 is not typically considered and was not applied in the present model. In fact, a number of inhibitors are thought to be converted to metabolites that meaningfully inhibit P450, such as verapamil and diltiazem. The impact of these processes on the estimation of shifted IC_{50} , and K_I and k_{inact} , has not been widely evaluated. Whereas further accuracy in inhibition parameters might be gained by modifying the model equations to account for them, a vastly larger data set is required to demonstrate applicability. For example, atypical inhibitor metabolism kinetics may be best characterized using metabolite formation experiments, which would require identification and quantification of all major metabolites of the inhibitor rather than inhibitor depletion as done currently. The impact of autoinhibition and autoinactivation on inhibitor-depletion kinetics requires knowledge of the fraction the inhibitor is metabolized by specific P450 in vitro. Finally, the impact of metabolite formation on the observed combined P450 inhibition requires proper characterization of each metabolite separately, which could themselves cause a combination of competitive or time-dependent inhibition. With this in mind, some assumptions must still be made, and a proper balance must be established between the desire for reasonably accurate inhibitor classification and parameter estimation and simplicity in experimental design.

In summary, the IC_{50} shift assay remains a viable approach to characterizing a wide range of reversible and time-dependent inhibitors. The value of the approach lies in the ability to evaluate both competitive and time-dependent inhibition in a single experiment. Further efficiencies are gained by omitting the dilution step found in traditional experimental designs and by using a substrate cocktail approach, which allows the evaluation of several P450s simultaneously. Anomalies, such as smaller-than-expected shift in IC_{50} and increases in IC_{50} with preincubation, were explained by depletion of inhibitor during the preincubation. As with traditional time-dependent inactivation methods, it is recommended that IC_{50} -shift experimental data be interpreted with knowledge of the extent of inhibitor depletion. For the most realistic classification of time-dependent inhibitors using IC_{50} -shift methods, shifted IC_{50} should be calculated using observed inhibitor concentrations at the end of the incubation rather than nominal inhibitor concentrations. Finally, a mechanistic model that includes key processes such as competitive inhibition, enzyme inactivation, and inhibitor depletion can be used to describe accurately observed IC_{50} and shifted IC_{50} curves. For compounds showing an IC_{50} fold shift >1.5 based on observed inhibitor concentrations, reanalyzing the IC_{50} -shift data using the mechanistic model appeared to allow for reasonable estimation of K_i , K_I , and k_{inact} directly from the IC_{50} shift experiments.

Acknowledgments

The authors thank Gary Skiles and Magang Shou for early discussions on the application and implementation of the IC_{50}/IC_{50} shift assay.

Authorship Contributions

Participated in research design: Berry, Zhao, Lin.

Conducted experiments: Berry.

Performed data analysis: Berry.

Wrote or contributed to the writing of the manuscript: Berry, Zhao, Lin.

References

- Albaugh DR, Fullenwider CL, Fisher MB, and Hutzler JM (2012) Time-dependent inhibition and estimation of CYP3A clinical pharmacokinetic drug-drug interactions using plated human cell systems. *Drug Metab Dispos* **40**:1336–1344.
- Berry LM and Zhao Z (2008) An examination of IC_{50} and IC_{50} -shift experiments in assessing time-dependent inhibition of CYP3A4, CYP2D6 and CYP2C9 in human liver microsomes. *Drug Metab Lett* **2**:51–59.
- Bertelsen KM, Venkatakrishnan K, Von Moltke LL, Obach RS, and Greenblatt DJ (2003) Apparent mechanism-based inhibition of human CYP2D6 in vitro by paroxetine: comparison with fluoxetine and quinidine. *Drug Metab Dispos* **31**:289–293.
- Burt HJ, Galetin A, and Houston JB (2010) IC_{50} -based approaches as an alternative method for assessment of time-dependent inhibition of CYP3A4. *Xenobiotica* **40**:331–343.
- Grimm SW, Einolf HJ, Hall SD, He K, Lim HK, Ling KH, Lu C, Nomeir AA, Seibert E, and Skordos KW, et al. (2009) The conduct of in vitro studies to address time-dependent inhibition of drug-metabolizing enzymes: a perspective of the pharmaceutical research and manufacturers of America. *Drug Metab Dispos* **37**:1355–1370.
- Ito K, Ogihara K, Kanamitsu S, and Itoh T (2003) Prediction of the in vivo interaction between midazolam and macrolides based on in vitro studies using human liver microsomes. *Drug Metab Dispos* **31**:945–954.
- Kenny JR, Mukadam S, Zhang C, Tay S, Collins C, Galetin A, and Khojasteh SC (2012) Drug-drug interaction potential of marketed oncology drugs: in vitro assessment of time-dependent cytochrome P450 inhibition, reactive metabolite formation and drug-drug interaction prediction. *Pharm Res* **29**:1960–1976.
- Kirby BJ, Collier AC, Kharasch ED, Whittington D, Thummel KE, and Unadkat JD (2011) Complex drug interactions of HIV protease inhibitors 1: inactivation, induction, and inhibition of cytochrome P450 3A by ritonavir or nelfinavir. *Drug Metab Dispos* **39**:1070–1078.
- Krippendorff BF, Neuhaus R, Lienau P, Reichel A, and Huisinga W (2009) Mechanism-based inhibition: deriving $K(I)$ and $k(inact)$ directly from time-dependent $IC(50)$ values. *J Biolom Screen* **14**:913–923.
- Li X, He Y, Ruiz CH, Koenig M, Cameron MD, and Vojtkovsky T (2009) Characterization of dasatinib and its structural analogs as CYP3A4 mechanism-based inactivators and the proposed bioactivation pathways. *Drug Metab Dispos* **37**:1242–1250.
- Maurer TS, Tabrizi-Fard MA, and Fung HL (2000) Impact of mechanism-based enzyme inactivation on inhibitor potency: implications for rational drug discovery. *J Pharm Sci* **89**:1404–1414.
- Mayhew BS, Jones DR, and Hall SD (2000) An in vitro model for predicting in vivo inhibition of cytochrome P450 3A4 by metabolic intermediate complex formation. *Drug Metab Dispos* **28**:1031–1037.
- Mori K, Hashimoto H, Takatsu H, Tsuda-Tsukimoto M, and Kume T (2009) Cocktail-substrate assay system for mechanism-based inhibition of CYP2C9, CYP2D6, and CYP3A using human liver microsomes at an early stage of drug development. *Xenobiotica* **39**:415–422.
- Obach RS, Walsky RL, and Venkatakrishnan K (2007) Mechanism-based inactivation of human cytochrome p450 enzymes and the prediction of drug-drug interactions. *Drug Metab Dispos* **35**:246–255.
- Perloff ES, Mason AK, Dehal SS, Blanchard AP, Morgan L, Ho T, Dandeneau A, Crocker RM, Chandler CM, and Boily N., et al. (2009) Validation of cytochrome P450 time-dependent inhibition assays: a two-time point IC_{50} shift approach facilitates kinact assay design. *Xenobiotica* **39**:99–112.
- Watanabe A, Nakamura K, Okudaira N, Okazaki O, and Sudo K (2007) Risk assessment for drug-drug interaction caused by metabolism-based inhibition of CYP3A using automated in vitro assay systems and its application in the early drug discovery process. *Drug Metab Dispos* **35**:1232–1238.
- Xu L, Chen Y, Pan Y, Skiles GL, and Shou M (2009) Prediction of human drug-drug interactions from time-dependent inactivation of CYP3A4 in primary hepatocytes using a population-based simulator. *Drug Metab Dispos* **37**:2330–2339.
- Yang J, Jamei M, Yeo KR, Tucker GT, and Rostami-Hodjegan A (2005) Kinetic values for mechanism-based enzyme inhibition: assessing the bias introduced by the conventional experimental protocol. *Eur J Pharm Sci* **26**:334–340.
- Yang J, Jamei M, Yeo KR, Tucker GT, and Rostami-Hodjegan A (2007) Theoretical assessment of a new experimental protocol for determining kinetic values describing mechanism (time)-based enzyme inhibition. *Eur J Pharm Sci* **31**:232–241.
- Zhao P, Kunze KL, and Lee CA (2005) Evaluation of time-dependent inactivation of CYP3A in cryopreserved human hepatocytes. *Drug Metab Dispos* **33**:853–861.
- Zhao P, Lee CA, and Kunze KL (2007) Sequential metabolism is responsible for diltiazem-induced time-dependent loss of CYP3A. *Drug Metab Dispos* **35**:704–712.

Address correspondence to: Loren M. Berry, Amgen, Inc., 360 Binney St., Cambridge, MA, 02142. E-mail: loren.berry@amgen.com